ARTICLE
Journal of Cellular Biochemistry 112:169–178 (2011)

Journal of Cellular Biochemistry

Sonodynamic Effects of Hematoporphyrin Monomethyl Ether on CNE-2 Cells Detected by Atomic Force Microscopy

Hua Jin,[1] Xing Zhong,[2] Zhiyong Wang,[3] Xun Huang,[1] Hongyan Ye,[1] Shuyuan Ma,[2] Yong Chen,[4**] and Jiye Cai[1*]

[1]*Department of Chemistry and Institute for Nano-Chemistry, Jinan University, Guangzhou 510632, China*
[2]*The First Affiliated Hospital, Medical College, Jinan University, Guangzhou 510632, China*
[3]*Department of Pathology, Medical College, Jinan University, Guangzhou 510632, China*
[4]*Institute for Advanced Study, Nanchang University, Nanchang, Jiangxi 330031, China*

ABSTRACT

Hematoporphyrin monomethyl ether (HMME) has been effectively used to treat solid tumors of some types. However, its application in nasopharyngeal carcinoma has not been studied yet. In this paper, the detailed sonodynamic effects of HMME-SDT (sonodynamic therapy) on CNE-2 cells including cell growth inhibition, apoptosis induction, and membrane toxicity were investigated. It was found that HMME alone had less cytotoxicity whereas HMME-SDT could suppress the cell proliferation in a dose-dependent manner as detected by MTT assay. The annexin V-based flow cytometric data indicated that upon SDT, different concentrations of HMME induce distinct types of cell death, apoptosis by low concentration (60 μg/ml) of HMME and necrosis by higher concentration (120 μg/ml). The immunofluorescence of cytoskeleton and nuclei morphology showed that upon HMME-SDT, the cells became rounding and the cytoskeletal network disappeared, and, the nuclei represented a total fragmented morphology of nuclear bodies. These alternations showed the apoptosis induction by HMME-SDT. Further AFM study showed that the cell membrane structure and cytoskeleton networks were destroyed, and, the Young's modulus, tip-cell-surface adhesion force decreased to 0.22 ± 0.11 Mpa, 35.4 ± 12.8 pN of cells with 120 μg/ml HMME-SDT from 0.48 ± 0.21 Mpa, 69.6 ± 22.3 pN of native cells, respectively. These membrane changes caused the collapse of mitochondrial transmembrane potential and disturbance of intracellular calcium homeostasis, which was consistent with the results detected by flow cytometry. Therefore, membrane toxicity and cytoskeleton disrupture induced by HMME-SDT maybe important factors to induce cell apoptosis, and, the disturbance of mitochondrial transmembrane potential and calcium channels might be the apoptosis mechanisms. J. Cell. Biochem. 112: 169–178, 2011.

KEY WORDS: SONODYNAMIC THERAPY; CNE-2 CELL; HEMATOPORPHYRIN MONOMETHYL ETHER; ATOMIC FORCE MICROSCOPY

Nasopharyngeal carcinoma (NPC) is a type of tumor arising from the epithelial cells that cover the surface of the nasopharynx. The tumor cells can translocate out of the nasopharynx to the other lateral wall and/or posterosuperiorly to the base of the skull or the palate, nasal cavity or oropharynx. It then typically metastases to cervical lymph nodes [Brennan, 2006]. NPC is very common in East Asia, Africa, southern regions of China [Fang et al., 2008]. The causes of the increasing risk for NPC in the above-mentioned areas are not entirely clear. So it is urgent to develop novel efficient, minimally invasive methods to treat this type of tumor.

Sonodynamic therapy (SDT) is based on photodynamic therapy (PDT) utilizing the photosensitive dyes that can be selectively retained by and accumulated in specific tissues or cells. In the presence of light irradiation, the dyes will produce reactive oxygen species (ROS) including singlet oxygen, hydroxyl radical, superoxide anions, etc. which lead to the destruction of the dye-containing cells but no damage to the surrounding, dye-free tissues,

Grant sponsor: National Natural Science Foundation of China; Grant number: 30900340; Grant sponsor: 973 program projects; Grant number: 2010CB833603.

*Correspondence to: Jiye Cai, Department of Chemistry and Institute for Nano-Chemistry, Jinan University, Guangzhou, China. E-mail: tjycai@jnu.edu.cn

**Correspondence to: Yong Chen, Institute for Advanced Study, Nanchang University, Nanchang, Jiangxi, China. E-mail: dr_yongchen@hotmail.com

Received 26 May 2010; Accepted 30 September 2010 • DOI 10.1002/jcb.22912 • © 2010 Wiley-Liss, Inc.
Published online 4 November 2010 in Wiley Online Library (wileyonlinelibrary.com).

or cells. Because of the limited penetrating depth of normal laser, PDT has mainly been adopted for the therapy of superficial cancers. Compared to laser, the ultrasound, especially focused ultrasound, can penetrate deeply into tissues and can be focused into a small region of tumors to activate the cytotoxicity of sonosensitizers [Yumita et al., 2003]. SDT has been regarded as one of the promising methods for cancer therapy.

Hematoporphyrin monomethyl ether (HMME) is the second generation of porphyrin-related photosensitizer, consisting of two monomer porphyrins, namely, 3-(1-methyloxyethyl)-8-(1-hydroxyethyl) deuteropor-phyrin IX and 8-(1-methyloxyethyl)-3-(1-hydroxyethyl) deuteropor-phyrin IX that are mutually locational isomers [Ding et al., 2004; Li et al., 2006]. HMME possesses some excellent properties, such as high selective uptake rate by tumor cells, strong photodynamic effect, low toxicity, and fast removal from organs or cells. Recently, HMME has been effectively used to treat solid tumors of some types [Ding et al., 2004; Kun et al., 2007]. However, the application in NPC has not been studied yet.

The cell membrane forms a barrier between the cell and the external environment and acts as the exchange interface of materials between the inside and outside of the cell [Marguet et al., 2006]. It plays key roles in the physiological processes of cells, such as cell adhesion, migration, signal transduction, and ion channel conductance [Muller, 2008]. So the changes in cell membrane structure can be a sensitive indicator of cell growth conditions. In the past decades, atomic force microscopy (AFM) has been extensively used to detect the morphological and biomechanical properties at molecular level. The ultra-high resolution imaging mode of AFM allows to obtain the images of cell morphology [Iscru et al., 2008], membrane ultrastructure [Muller, 2008; Wang et al., 2009], nuclear pores [Oberleithner et al., 1994], even single membrane proteins peppering a cellular membrane [Fotiadis et al., 2003]. And, the force spectroscopy can be used to detect the dynamic processes-correlated cellular and molecular biomechanics, such as stiffness (or Young's) modulus [Cross et al., 2007; Stolz et al., 2009; Jin et al., 2010], specific [Hinterdorfer and Dufrêne, 2006] and nonspecific adhesion forces [Abu-Lail and Camesano, 2006].

In this paper, the interactions of NPC cell line CNE-2 cells with photosensitizer HMME were characterized using MTT assay, flow cytometry, immunefluorescence, and AFM-based technology. Our data in vitro proved that HMME-SDT could be as a novel therapic method to treat the human NPC cell Line CNE-2 cells.

MATERIALS AND METHODS

CHEMICALS

HMME (10 mg/ml) was purchased from Shanghai Red-Green Photosensitizer, Co., China. Rhodamin 123 and Fluo-3 AM were purchased from Beyotime Institute of Biotechnology, China. All reagents used in the experiments were of analytical grade.

CELL LINE AND CULTURE

Human NPC cell line CNE-2 was obtained from Biochemistry laboratory, The First Affiliated Hospital of Jinan University. Cells were cultured in RPMI-1640 medium (Gibco) supplemented with 10% fetal calf serum (Gibco) in an incubator (5% CO_2, 37°C), and the medium was freshed every 2–3 days. Cells were harvested with 0.25% trypsin (Gibco) when needed.

SONODYNAMIC EXPERIMENTS

The frequency of ultrasound was 1.0 MHz, the acoustic intensity 1.5 W cm^{-2}, and the exposure time 60 s. Four experimental groups were designed: a, no treatment; b, HMME (10 or 60 or 120 μg/ml) treatment; c, ultrasound treatment; d, combination of HMME and ultrasound treatment (HMME-SDT). In each group, cells were separated into two parts, one for AFM measurement and the other for MTT assay.

MTT ASSAY

The CNE-2 cells for MTT assay were transferred into the wells of 96-well plates at a density of 10^6 cells/ml, followed by addition of 100 μl MTT (3-(4, 5-dimethyl-2-thiazolyl)-2,5-diphenyl tetrazolium bromide). All these operations were performed in dark. Then, the plates were incubated in humidified air at 37°C with 5% CO_2 for 4 h. The optical density of the colored product was measured at 570 nm using a BioRad microplate reader. Cytotoxity (IC_{50}) data were analyzed using the GraphPad computer software.

DETERMINATION OF APOPTOSIS RATE

An Annexin V-FITC/PI apoptosis detection kit was used to detect early apoptotic activity according to the manufacturer's instructions. After sonodynamic treatments, CNE-2 cells were washed with cold PBS and suspended in 500 μl Annexin V binding buffer. After stained twice with 5 μl FITC labeled-Annexin V and 5 μl PI, and incubated for 30 min at room temperature in the dark, the samples were immediately analyzed by a flow cytometer (BD FACSAria™).

MEASUREMENTS OF MITOCHONDRIAL MEMBRANE POTENTIAL (MMP) AND CYTOSOLIC FREE CALCIUM LEVELS

To detect the changes in MMP and cytosolic free calcium levels, the CNE-2 cells treated with HMME-SDT at designated concentrations were incubated with rhodamin 123 and Fluo-3 AM for 30 min in dark at room temperature, separately. The cells were collected and washed twice with PBS. The resulting fluorescence was measured by the flow cytometer.

IMMUNOFLUORESCENT STAINING

The characterizations of apoptosis and cytoskeleton were evaluated by staining with DAPI and rhodamine–phalloidin, separately. The CNE-2 cells with or without HMME-SDT treatments were fixed with 4% paraformaldehyde for 30 min and incubated with 50 μM of DAPI and 1 μM rhodamine–phalloidin for 60 min in the dark at room temperature, separately. After that, the cells were washed twice with PBS. Then, the nuclear morphology and organization of cytoskeleton were imaged by a laser scanning confocal microscope (LCM 510 Meta Duo Scan, Carl Zeiss, Germany).

SINGLE CELL AFM MEASUREMENT

An AFM (Autoprobe CP Research, Veeco, USA) was used in the contact mode to obtain topographic images. The silicon nitride tips (UL20B; Park Scientific Instruments) used in all AFM measurements

were irradiated with ultraviolet in air for 15 min to remove any organic contaminates prior to use. The curvature radius of the tips is <10 nm, and the length, width, and thickness of the cantilevers are 115, 30, and 3.5 μm, respectively, with an oscillation frequency of 255 kHz and a force constant of 0.01 N/m (manufacture offered).

After initial scanning of the cell surface, various locations on a cell were selected for obtaining the force–distance curves by the force-modulate mode AFM. All force–distance (F–D) curve experiments were performed at the same loading rate. The Young's modulus calculations were done based on the basic Hertz model which shows the relationship between the applied force F and the indentation δ (shown in the following equation):

$$F = \frac{4}{3}\frac{ER^{1/2}\delta^{3/2}}{(1-\upsilon^2)}$$

where ν is the poisson ratio, F the loading force, δ the indentation, E the Young's modulus, and R the curvature radius of the AFM tip, respectively. A Poisson ratio of 0.5 is appropriate for lipid bilayers, cells, and vesicles [Laney et al., 1997; Radmacher, 2002; Liang et al., 2004].

STATISTICAL ANALYSIS

Single-cell imaging was performed on more than five cells, and each cell was scanned for three times. F–D curves are calculated using the standard formula. All data were average values ± SD of more than 150 F–D curves, taken from 5 to 10 different cells. Statistical analysis was performed using Student's t-test, with $P < 0.05$ regarded as statistically significant.

RESULTS AND DISCUSSIONS

HMME-SDT EFFECTS ON THE GROWTH OF CNE-2 CELLS

The cytotoxicity of HMME-SDT effects were assessed by MTT assays. The results (shown in Fig. 1A) revealed that there was no significant cell damage observed in the cells treated with HMME alone or ultrasound alone, implying that HMME or ultrasound alone had no intrinsic cytotoxicity. However, in combination with ultrasound treatment (1MHz, 1.5 W/cm^2 × 60 s), HMME had a dose-dependent killing effect on the CNE-2 cells, and 120 μg/ml HMME-SDT killed over 90% cells.

APOPTOSIS-INDUCING EFFECTS OF HMME-SDT

To further assess the apoptotic cells induced by HMME-SDT, flow cytometric analysis of the CNE-2 cells labeled with FITC-annexin V was performed. As seen in Figure 1B, Q4 represented the early apoptosis of cells, and Q2 represented the necrosis of cells. With 60 μg/ml HMME-SDT treatment, the number of apoptotic cells was higher than that of necrotic cells. Nevertheless, with 120 μg/ml HMME-SDT, the number of necrotic cells was significant higher than that of apoptotic cells. It suggests that upon SDT, different concentrations of HMME induce distinct types of cell death, apoptosis by low concentration of HMME and necrosis by higher concentration.

CHANGES IN MITOCHONDRIAL MEMBRANE POTENTIAL (MMP)

Evaluation of the toxicity-induced MMP loss plays an important role in screening drug candidates. With mitochondrial damage or loss of MMP, rhodamin 123 cannot accumulate in the mitochondria, which is indicated by a decrease of mean fluorescence intensity (MFI). As shown in Figure 2B,C, there is a significant decrease of MFI in CNE-2 cells compared with that of control group (Fig. 2A), which indicated that the rapid drop in MMP induced by HMME-SDT. Due to the disruption of the outer membrane induced by HMME-SDT, the permeability transition pore was opened or the voltage-dependent anion channels in the mitochondrial outer membrane were closed, and these alternations may result in the remarkable loss of MMP.

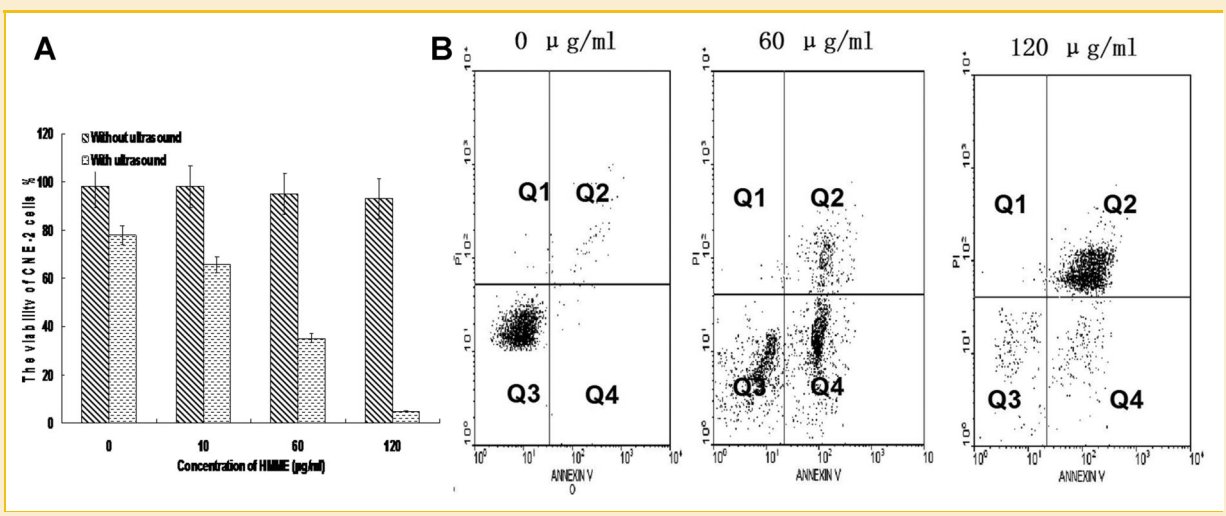

Fig. 1. A: Histogram of the cell viability of CNE-2 cells treated by different concentrations of HMME with or without exposing to ultrasound measured by MTT assay. The results reveal that only the sonodynamic-treated CNE-2 cells were killed by HMME in a dose-dependent manner. B: Flow cytometric analysis of the apoptosis of the CNE-2 cells treated with different concentrations of HMME. The Q4 quadrant represents the apoptotic target cells and the Q2 quadrant represents the necrotic cells.

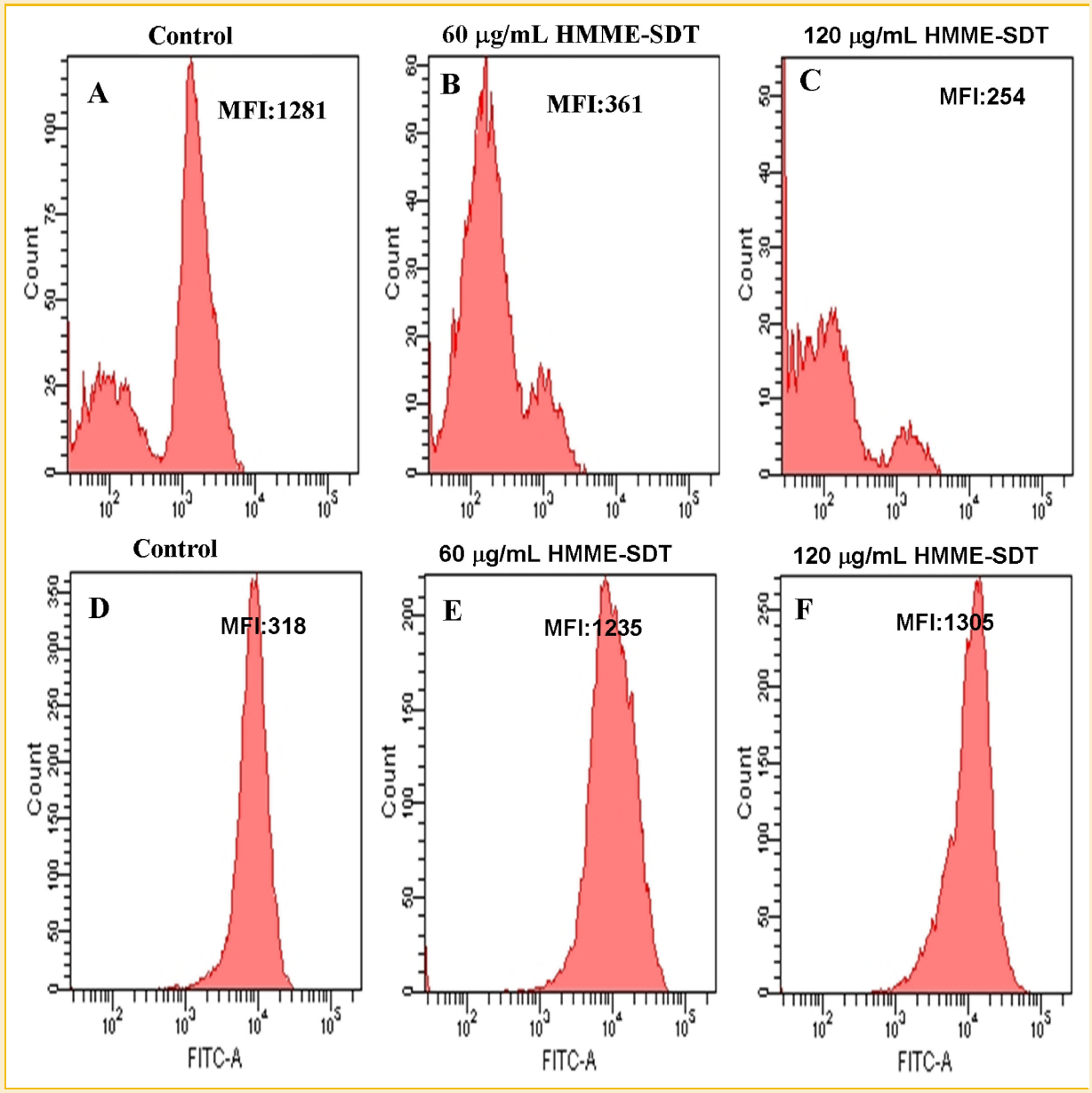

Fig. 2. Flow cytometric analysis of MMP (A–C) and intracellular Ca^{2+} level (D–F) in CNE-2 cells treated with designated concentrations of HMME-SDT. The resulting fluorescence MFI was the indicator of MMP or intracellular Ca^{2+} levels. The significant reduction of MMP or increase of intracellular Ca^{2+} levels indicated that HMME-SDT treatments could induce CNE-2 cell apoptosis at a large scale. [Color figure can be viewed in the online issue, which is available at wileyonlinelibrary.com.]

Previous studies have reported that MMP loss could lead to cytochrome c release and caspases activation (Waterhouse et al., 2001), which play important roles in the induction of apoptosis. Therefore, HMME-SDT-induced loss of MMP should play key roles in the apoptosis of CNE-2 cells.

INTRACELLULAR FREE CA^{2+} DETECTION

Intracellular calcium regulates a wide range of vital cell functions, such as cell growth and proliferation and signal-transduction. We therefore measured the intensity of intracellular fluo-3 fluorescence, an indicator of Ca^{2+} level, in CNE-2 cells before and after treatment with HMME-SDT. As Figure 2D–F shown, intracellular calcium of cells treated with HMME-SDT increased significantly than that of control cells.

Prolonged elevation of intracellular free Ca^{2+} level will trigger diverse abnormal cellular processes, even apoptosis. Cell signaling can be activated by a temporary increase in intracellular calcium level through the opening of calcium channels in the plasma membrane or the endoplasmic reticulum. The rise in intracellular Ca^{2+} level induced by HMME-SDT might be largely associated with the collapse of membrane integrity (Fig. 4), which could induce the opening of Ca^{2+} channels in cell membrane and the consequent influx of Ca^{2+}.

IMMUNOFLUORESCENCE

The control cells presented a spindle-like shape and grew in clones (Fig. 3A), but after HMME-SDT treatment, the cells became retracted and contractive (Fig. 3B,C). Previous studies have shown that cytoskeleton alterations could induce apoptosis in a variety of model [White et al., 2001; Kulms et al., 2002; Genesca et al., 2006]. So, it was important to detect the HMME-SDT effects on the arrangement of F-actins. Figure 3D–F showed the reorganization of F-actins in CNE-2 cells by staining with rhodamine–phalloidin. The assembly of actins in control cells represented regular mesh-networks (Fig. 3D), however, after HMME-SDT treatments, the cells became shrinking and rounding, the cytoskeletal networks disappeared, and the cell integrity was damaged (Fig. 3E,F).

Moreover, the apoptosis assay was performed using DAPI staining. When DAPI binds to natural double-stranded DNAs, the fluorescence is strongly enhanced and the morphology of the nuclei can be clearly visualized, based on which the apoptotic cells can be identified. Figure 3G–H showed the representative nuclei morphology in the DAPI-stained CNE-2 cells treated with 60 μg/ml HMME-SDT. There were intact, plump nuclei in control cells (white arrows in Fig. 3G). While, the nuclei of apoptotic cells represented a total fragmented morphology of nuclear bodies and the condensed chromatin gathering at the periphery of the nuclear membrane (gray arrows in Fig. 3G). This indicated that HMME-SDT could significantly inhibit proliferation and induce apoptosis of CNE-2 cells.

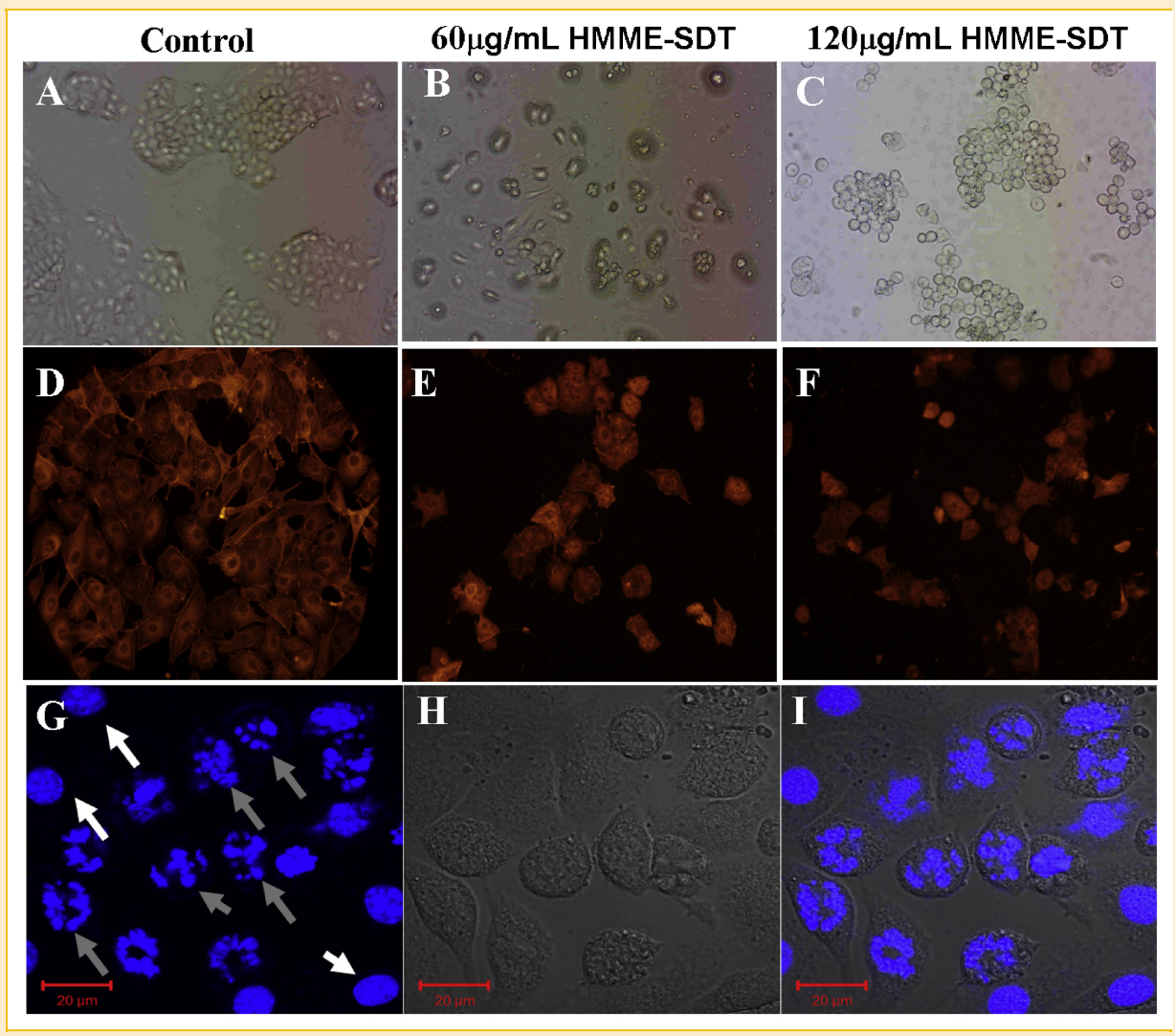

Fig. 3. Morphological data of CNE-2 cells treated with the designated concentrations of HMME-SDT. A–C: Changes in morphology observed under a phase microscope. D–F: The reorganization of cytoskeleton in cells stained with Rhodamine–phalloidin. G–I: Nuclei of normal and apoptotic cells stained with DAPI. The fluorescence image, the phase image, and the merged one are shown in G–I, respectively. In figure G, the white arrows indicate the normal cells; and the gray arrows show the apoptotic cells. After HMME-SDT, the cells became shrinking and rounding (B,C), the cytoskeleton networks disappeared (E,F), and the nuclei staining represented fragmented morphology of nuclear bodies, which indicated the apoptosis induction by HMME-SDT. [Color figure can be viewed in the online issue, which is available at wileyonlinelibrary.com.]

Taken together, these data indicated that cytoskeleton reorganization and DNA fragmentations in CNE-2 cells might be killing pathways of HMME-SDT.

AFM ANALYSIS

Changes in cell morphology. As a nondestructive surface imaging tool, AFM can obtain images of cell surface at the molecular level which can provide us important details on the architecture of cell membranes. In this work, the tapping mode AFM was used for cell scanning and to observe a variety of changes in surface morphology and ultrastructure of CNE-2 cells treated with different concentrations of HMME-SDT.

Figure 4 showed AFM images of CNE-2 cells. Control cells had a regular spindle or oval shape, and the cell surface was relatively smooth and intact (A,B). Figure 4C,D were the CNE-2 cells treated with 120 μg/ml HMME treatment alone, and, no remarkable changes in cell surface were observed. In Figure 4C,D, we can see a dividing cell, in which two unseparated daughter cells are evident, indicating that HMME has low intrinsic cytotoxicity and has no effects on cell growth and proliferation of CNE-2 cells. But, on cells treated with 60 μg/ml HMME-SDT, the morphological changes, such as blebbing, pores, and apoptotic bodies were observed (Black arrows shown in E,G). And these characteristics were similar to the symbols of apoptosis. Significant shrinkage and deep pores, however, which were similar to the symbols of necrosis, emerged on the cell surface (Black arrows shown in Fig. 4I–L) when treated with 120 μg/ml HMME-SDT.

Simultaneously, AFM can reveal the alternations of cell surface ultrastructure at nanometer scale. Figure 5 showed the ultrastructural data of CNE-2 cells. The cell membrane architecture of control cells (Fig. 5A–D) was homogeneous and represented granular morphology with the surface particles of around 400 nm. Figure 5E–H showed the cell surface architecture of CNE-2 cells with HMME-SDT treatment. The height profile of located area was in a wavy shape and the architecture became heterogeneous. And, the sizes of the membrane particles on CNE-2 cells treated with 60 and 120 μg/ml HMME-SDT were 160 and 50 nm, respectively (Fig. 5F,I). Moreover, the cytoskeleton structure of control cell presented regular networks of F-actins (shown in Fig. 5A), while after HMME-SDT treatment, the cytoskeleton networks disappeared, and the number of F-actins significantly decreased (shown in Fig. 5E,I).

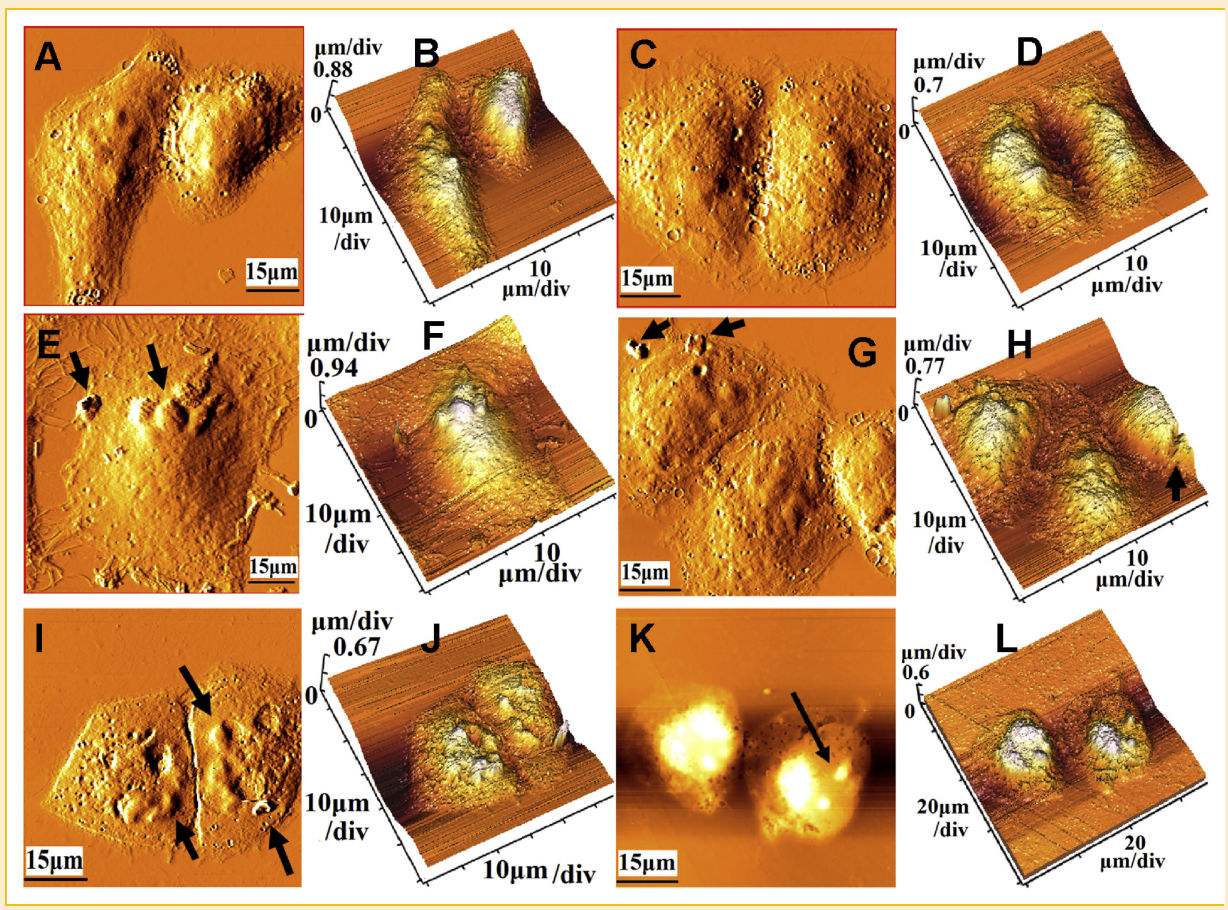

Fig. 4. AFM topographic data of CNE-2 cells. A: Native CNE-2 cells. C: CNE-2 cells incubated with 120 μg/ml HMME in dark. These images indicate that there are no significant changes appeared on the cell surface treated with HMME alone. E,G: CNE-2 cells treated with 60 μg/ml HMME-SDT. The morphological characteristics are similar to the symbol of cell apoptosis. I,K: CNE-2 cells treated with 120 μg/ml HMME-SDT. The morphological characteristics are indications of the cell necrosis. B,D,F,H,J,L are the 3D mode of A,C,E,G,I,K, respectively. Scanning area: (A–H) $50 \times 50\ \mu m^2$, (I,J) $55 \times 55\ \mu m^2$, (K,L) $65 \times 65\ \mu m^2$. [Color figure can be viewed in the online issue, which is available at wileyonlinelibrary.com.]

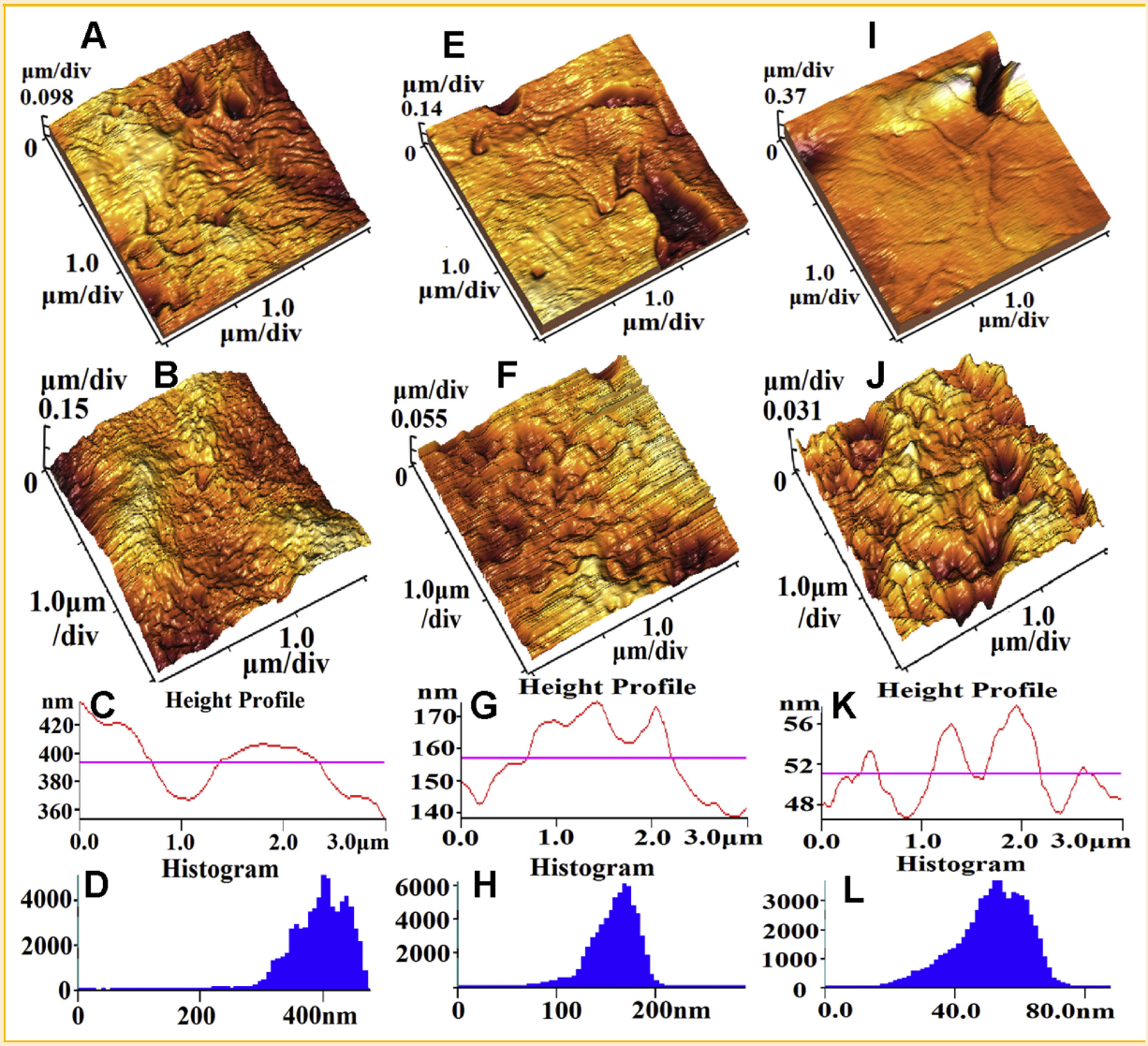

Fig. 5. AFM ultrastructural data of CNE-2 cells: (A–D) native cells, (E–H) cells treated with 60 μg/ml HMME-SDT. I–L: CNE-2 cells treated with 120 μg/ml HMME-SDT. A,E,I: Cytoskeleton structure. B,F,J: Ultrasructure of cell membrane. C,G,K: Height profiles, (D,H,L) histograms of the particle size extracted from images B, F, and J, respectively. Scanning area: $3 \times 3\ \mu m^2$. With the concentration of HMME-SDT increasing, the cytoskeleton networks disappeared, and the number of F-actins significantly decreased. [Color figure can be viewed in the online issue, which is available at wileyonlinelibrary.com.]

Furthermore, the roughness of cell membrane is directly or indirectly sensitive to the membrane-skeleton integrity[Girasole et al., 2007]. In each group of cells, we choose 20 different local regions ($3 \times 3\ \mu m^2$) for Ra measurement. The statistical results indicate that the Ra values of CNE-2 cells treated with 60, 120 μg/ml are 254.46 ± 58.74, 121.84 ± 22.35 nm, respectively, which are significant lower than that of control cells (287.98 ± 88.06 nm).

Taken together, all these morphological data revealed that there were dose-dependant changes in morphological data of cells treated with HMME-SDT. And, low concentration (60 μg/ml) of HMME-SDT mainly induced cell apoptosis, high concentration (120 μg/ml) of HMME-SDT primarily induced cell necrosis. Especially, the alternations in ultrastructure of cytoskeleton and membrane surface might result from the altered chemical composition of the outer membrane. This provided more detailed information for understanding the membrane toxicity induced by HMME-SDT.

Nanomechanical alternations detected by AFM. It's difficult to interpret the mechanisms of HMME-SDT effects on CNE-2 cells only based on the morphological data. To get more detailed information, force measurements were performed to investigate the compositional changes of the cell surface at molecular level. The alternations in biomechanical properties of CNE-2 cells induced by HMME-SDT were shown in Figure 6.

Stiffness or elasticity of cells have been identified as important factors relating to cell function, adherence, motility, transformation, and invasion (Cross et al., 2008). Figure 6D showed the changes in stiffness (Young's modulus) of CNE-2 cells before and after HMME-SDT treatment. The statistical results indicated that the Young's modulus of cells treated with 60 and 120 μg/ml HMME-SDT notably

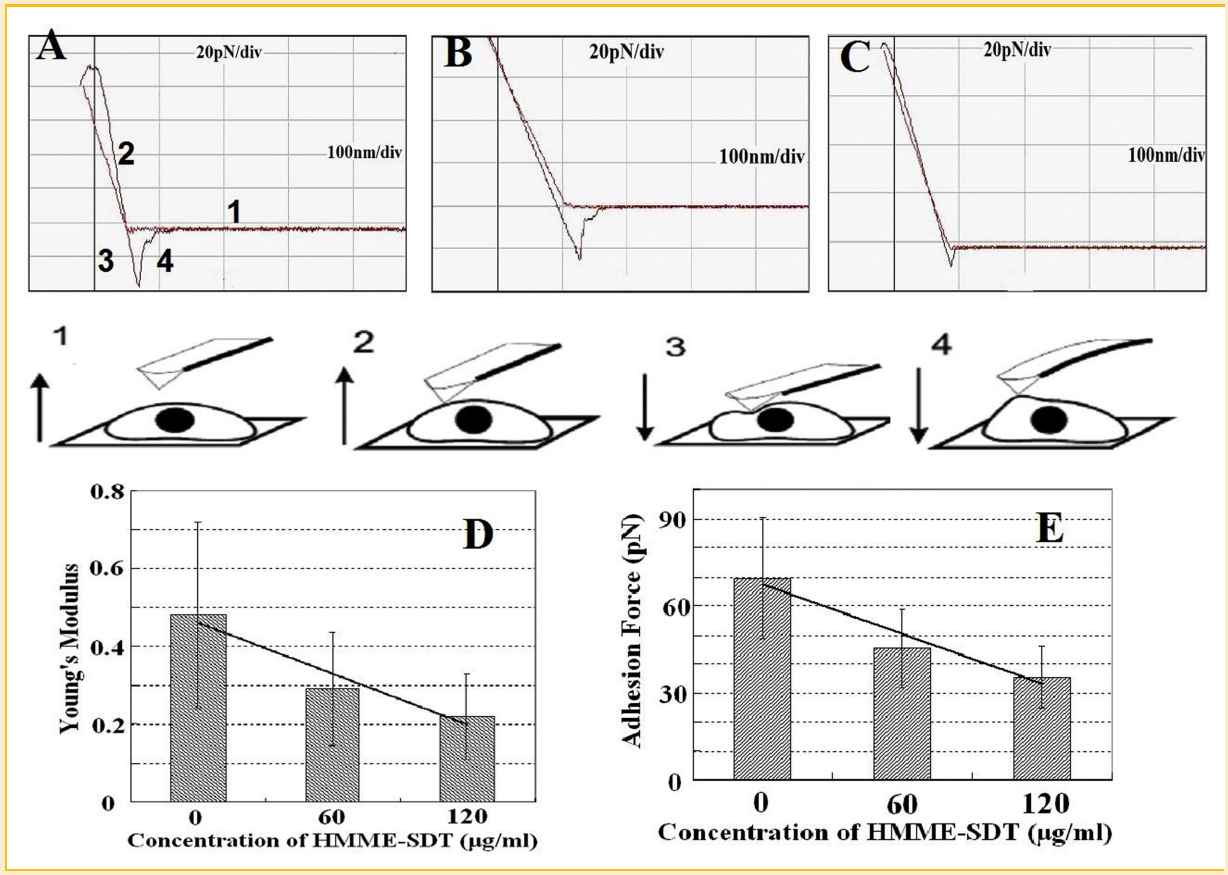

Fig. 6. AFM mechanical data of CNE-2 cells treated with HMME-SDT. Typical force–distance curves of control CNE-2 cell (A), CNE-2 cell treated with 60 μg/ml HMME-SDT (B), and CNE-2 cell treated with 120 μg/ml HMME-SDT (C). The middle panel illustrates an approach (frames 1–3)–retraction (frame 4) cycle. D, E are histograms of Young's modulus and adhesion force of CNE-2 cells treated with different concentrations of HMME-SDT. With the concentration of HMME increasing, the Young's modulus and adhesion forces both decreased significantly compared with those of native cells. [Color figure can be viewed in the online issue, which is available at wileyonlinelibrary.com.]

reduced from 0.48 ± 0.21 Mpa of control cells to 0.29 ± 0.12 and 0.22 ± 0.11 Mpa, respectively. The significantly decrease in Young's modulus might be due to the HMME-SDT-induced damages to cytoskeleton. With the irradiation of visible light or ultrasound treatment, the photosensitizer can drive molecular oxygen into excited triplet state transferring energy into ground state molecular oxygen, which produces singlet molecular oxygen. Increased level of activated singlet oxygen, or ROS in general, may strongly influence the polymerization of actin fibers [Moldovan et al., 2000; Dalle-Donne et al., 2001], and lead to dramatic changes in cytoskeleton reorganization. The reorganization of cytoskeleton and decrease in number of F-actins lead to the largely drop of membrane rigidity, which were consistent with the morphological images of cytoskeleton (shown in Fig. 5E,I).

Additionally, it has been proved that changes in adhesion of live cells to external substrates [Geiger, 2001] are involved in many cellular processes, including cell growth, differentiation, motility, and apoptosis [Giancotti and Ruoslahti, 1999]. Figure 6E indicated that the cell-surface adhesion forces of CNE-2 cells treated with 60 and 120 μg/ml HMME-SDT were 45.3 ± 17.5 and 35.4 ± 12.8 pN, respectively, which were notably reduced compared with that of the control cells (69.6 ± 22.3 pN). It perhaps resulted from the damages of cell surfaces or the changes in cell membrane composition induced by SDT. The nonspecific adhesion forces of cells can be as a function of the nanomechanical properties of the existing surface adhesive molecules. The damage to the cellular structural elements, like the cell membrane, transmembrane proteins, or focal adhesion points, may lead to the decreases in the number of the existing surface adhesive molecules. Another possibility may result from the changes in the number of microvilli on the cell surface. As Tang et al. [2008] reported, there was a significant decrease in the number of microvilli on the sarcoma 180 cell surface after exposure to sonoactivated hematoporphyrin. And, the decreases in Ra of cells treated with HMME-SDT also confirm the verdict.

Taken together, our morphological and biomechanical data detected by AFM showed that the stiffness and adhesion force properties of CNE-2 cells can be altered by HMME-SDT, and, AFM can be as a convenient and sensitive nanodevice for studying the interactions between cells and drugs.

CONCLUSIONS

In this paper, we investigated the in situ HMME-SDT effects on CNE-2 cells using MTT assay, flow cytometry, immunefluorescence, and AFM-based technology. The AFM morphological data and

annexin V-based flow cytometric data indicated that HMME-SDT could effectively induce apoptosis of CNE-2 cells in a dose-dependent manner, and, different concentrations of HMME induced different types of cell death, apoptosis (low concentration of HMME), or necrosis (high concentration). Also, the alternations in the immunofluorescence of cytoskeleton and nuclei morphology also showed the apoptosis induction by HMME-SDT. These data proved that HMME-SDT could be as a novel therapic method to treat the human NPC cell Line CNE-2 cells.

To further confirm the results and figure out the mechanism, we detected the changes in cell topography, membrane surface ultrastructure, cytoskeleton architecture, cell stiffness, and membrane adhesion, using AFM. The results indicated that the HMME-SDT-induced damage of cell membrane had a certain positive correlation with the concentration of HMME. Upon HMME-SDT treatment, ultrastructure of cell surface changed from a homogeneous to a heterogenous morphology and there were shrinkage and pores appeared on the cell surface. And, the cytoskeleton networks disappeared, and the number of F-actins decreased significantly after HMME-SDT. Moreover, the nanomechanical data indicated that after sonodynamic treatment, the cell surface became less rigid and adhesive. The Young's modulus, tip-cell-surface adhesion force decreased to 0.22 ± 0.11 Mpa, 35.4 ± 12.8 pN of cells with 120 μg/ml HMME-SDT from 0.48 ± 0.21 Mpa, 69.6 ± 22.3 pN of native cells, respectively. It was speculated that the HMME-SDT induced the changes in the chemical composition of the cell surface and the decrease in the number of microvilli and actins on the cell surface. All these alternations indicated the membrane structure was disrupted by HMME-SDT. Simultaneously, the collapse of MMP and the rapid increase of cytosolic free Ca^{2+} detected by flow cytometry further confirmed that the apoptosis induction was resulted from the membrane toxicity induced by HMME-SDT.

These experiments, revealing that the membrane toxicity and cytoskeleton disrupture may be the therapic targets of HMME-SDT, contribute to shedding new light into the structure–function relationships of cell surfaces and understanding the mechanisms of the interactions between cells and drugs. And, the AFM ability to detect the subtle changes at the nanometer scale in structural and biomechanical properties of cancer cells before and after treatment with drugs has opened up the exciting prospect of using simple nanodevice as a potential sensitive tool.

ACKNOWLEDGMENTS

We express our thanks to Prof. Guanqun Yang (The First Affiliated Hospital, Jinan University, China), Zhihong Liang, Yaping Yang, and Xingqiang Lai (Analytical & Testing Center, Jinan University, China) for their help and hot discussion.

REFERENCES

Abu-Lail NI, Camesano TA. 2006. Specific and nonspecific interaction forces between *Escherichia coli* and silicon nitride, determined by poisson statistical analysis. Langmuir 22(17):7296–7301.

Brennan B. 2006. Nasopharyngeal carcinoma. Orphanet J Rare Dis 1:23.

Cross SE, Jin YS, Tondre J, Wong R, Rao JY, Gimzewski JK. 2007. Nanomechanical analysis of cells from cancer patients. Nat Nanotechnol 2:780–783.

Dalle-Donne I, Rossi R, Milzani A, Simplicio PD, Colombo R. 2001. The actin cytoskeleton response to oxidants: From small heat shock protein phosphorylation to changes in the redox state of actin itself. Free Radic Biol Med 31(12):1624–1632.

Ding X, Xu Q, Liu F, Zhou P, Gu Y, Zeng J, An J, Dai W, Li X. 2004. Hematoporphyrin monomethyl ether photodynamic damage on HeLa cells by means of reactive oxygen species production and cytosolic free calcium concentration elevation. Cancer Lett 216(1):43–54.

Fang W, Li X, Jiang Q, Liu Z, Yang H, Wang S, Xie S, Liu Q, Liu T, Huang J, Xie W, Li Z, Zhao Y, Wang E, Marincola FM, Yao K. 2008. Transcriptional patterns, biomarkers and pathways characterizing nasopharyngeal carcinoma of Southern China. J Transl Med 6:32–44.

Fotiadis D, Liang Y, Filipek S, Saperstein DA, Engel A, Palczewski K. 2003. Atomic-force microscopy. Rhodopsin dimers in native disc membranes. Nature 421:127–128.

Geiger B. 2001. Cell biology: Encounters in space. Science 294:1661–1663.

Genescà M, Sola A, Hotter G. 2006. Actin cytoskeleton derangement induces apoptosis in renal ischemia/reperfusion. Apoptosis 11:563–571.

Giancotti FG, Ruoslahti E. 1999. Integrin signaling. Science 285:1028–1033.

Girasole M, Pompeo G, Cricenti A, Congiu-Castellano A, Andreola F, Serafino A, Frazer BH, Boumis G, Amiconi G. 2007. Roughness of the plasma membrane as an independent morphological parameter to study RBCs: A quantitative atomic force microscopy investigation. Biochim Biophys Act Biomembr 1768:1268–1276.

Hinterdorfer P, Dufrêne YF. 2006. Detection and localization of single molecular recognition events using atomic force microscopy. Nat Methods 3:347–355.

Iscru DF, Anghelina M, Agarwal S, Agarwal G. 2008. Changes in surface topologies of chondrocytes subjected to mechanical forces: An AFM analysis. J Struct Biol 162(3):397–403.

Jin H, Xing X, Zhao H, Chen Y, Huang X, Ma S, Ye H, Cai J. 2010. Detection of erythrocytes influenced by aging and type 2 diabetes using atomic force microscope. Biochem Biophys Res Commun 391(4):1698–1702.

Kulms D, Düssmann H, Pöppelmann B, Ständer S, Schwarz A, Schwarz T. 2002. Apoptosis induced by disruption of the actin cytoskeleton is mediated via activation of CD95 (Fas/APO-1). Cell Death Differ 9:598–608.

Laney D, Garcia R, Parsons S, Hansma H. 1997. Changes in the elastic properties of cholinergic synaptic vesicles as measured by atomic force microscopy. Biophys J 72(2):806–813.

Li P, Sun JG, Huang CR, Pan GY, Xu MJ, Li J, Wang GJ, Tao JN. 2006. Development and validation of a sensitive quantification method for hematoporphyrin monomethyl ether in plasma using high-performance liquid chromatography with fluorescence detection. Biomed Chromatogr 20:1277–1282.

Liang X, Mao G, Simon Ng KY. 2004. Probing small unilamellar EggPC vesicles on mica surface by atomic force microscopy. Colloids Surf B Biointerfaces 34(1):41–51.

Marguet D, Lenne PF, Rigneault H, He HT. 2006. Dynamics in the plasma membrane: How to combine fluidity and order. EMBO J 25:3446–3457.

Moldovan L, Moldovan NI, Sohn RH, Parikh SA, Goldschmidt-Clermont PJ. 2000. Redox changes of cultured endothelial cells and actin dynamics. Circ Res 86:549–557.

Muller DJ. 2008. AFM: A nano tool in membrane biology. Biochemistry 47(31):7986–7998.

Oberleithner H, Brinckmann E, et al. 1994. Imaging nuclear pores of aldosterone-sensitive kidney cells by atomic force microscopy. Natl Acad Sci 91:9784–9788.

Radmacher M. 2002. Measuring the elastic properties of living cells by the atomic force microscope. Methods Cell Biol 68:67–90.

Song K, Kong B, Li L, Yang Q, Wei Y, Qu X. 2007. Intraperitoneal photodynamic therapy for an ovarian cancer ascite model in Fischer 344 rat using hematoporphyrin monomethyl ether. Cancer sci 98:1959–1964 .

Stolz M, Gottardi R, Raiteri R, Miot S, Martin I, Imer R, Staufer U, Raducanu A, Düggelin M, Baschong W, Daniels AU, Friederich NF, Aszodi A, Aebi U. 2009. Early detection of aging cartilage and osteoarthritis in mice and patient samples using atomic force microscopy. Nat Nano 4(3):186–192.

Tang W, Liu Q, Wang X, Mi N, Wang P, Zhang J. 2008. Membrane fluidity altering and enzyme inactivating in sarcoma 180 cells post the exposure to sonoactivated hematoporphyrin in vitro. Ultrasonics 48(1):66–73.

Wang J, Wan Z, Liu W, Li L, Ren L, Wang X, Sun P, Ren L, Zhao H, Tu Q, Zhang Z, Song N, Zhang L. 2009. Atomic force microscope study of tumor cell membranes following treatment with anti-cancer drugs. Biosens Bioelectron 25(4):721–727.

Waterhouse NJ, Goldstein JC, von Ahsen O, Schuler M, Newmeyer DD, Green DR. 2001. Cytochrome c maintains mitochondrial transmembrane potential and ATP generation after outer mitochondrial membrane permeabilization during the apoptotic process. J Cell Biol 153:319–328.

White SR, Williams P, Wojcik KR, Sun S, Hiemstra PS, Rabe KF, Dorscheid DR. 2001. Initiation of apoptosis by actin cytoskeletal derangement in human airway epithelial cells. Am J Respir Cell Mol Biol 24:282–294.

Yumita N, Umemura S. 2003. Sonodynamic therapy with photofrin II on AH130 solid tumor. Cancer Chemother Pharmacol 51(2):174–178.